

Hydrogen spillover and storage on graphene with single-site Ti catalysts

Jih-Wei Chen^{1,2,#}, Shang-Hsien Hsieh^{2,#}, Sheng-Shong Wong^{1,#}, Ya-Chi Chiu¹, Hung-Wei Shiu², Chia-Hsin Wang², Yaw-Wen Yang², Yao-Jane Hsu², Domenica Convertino³, Camilla Coletti³, Stefan Heun⁴, Chia-Hao Chen^{2*}, and Chung-Lin Wu^{1,2*}

¹Department of Physics, National Cheng Kung University, Tainan 70101, Taiwan

²National Synchrotron Radiation Research Center, Hsinchu 30076, Taiwan

³Center for Nanotechnology Innovation @ NEST, Istituto Italiano di Tecnologia, Pisa 56127, Italy

⁴NEST, Istituto Nanoscienze-CNR and Scuola Normale Superiore, 56127 Pisa, Italy

[#]Contributed equally

*Correspondence and requests for materials should be addressed to C.-H. Chen and C.-L Wu

(E-mail: chchen@nsrrc.org.tw and clwuphys@mail.ncku.edu.tw)

Abstract

Hydrogen spillover and storage for single-site metal catalysts, including single-atom catalysts (SACs) and single nanocluster catalysts, have been elucidated for various supports but remain poorly understood for inert carbon supports. Here, we use synchrotron radiation-based methods to investigate the role of single-site Ti catalysts on graphene for hydrogen spillover and storage. Our *in-situ* angle-resolved photoemission spectra results demonstrate a bandgap opening and the X-ray absorption spectra reveal the formation of C–H bonds, both indicating the partial graphene hydrogenation. With increasing Ti deposition and H₂ exposure, the Ti atoms tend to aggregate to form nanocluster catalysts and yield 13.5% *sp*³-hybridized carbon atoms corresponding to a hydrogen-storage capacity of 1.11 wt% (excluding the weight of the Ti nanoclusters [1]). Our results demonstrate how a simple spillover process at Ti SACs can lead to covalent hydrogen bonding on graphene, thereby providing a strategy for a rational design of carbon-supported single-site catalysts.

Chemical catalytic reactions involving hydrogen, which are ubiquitous in the chemical industry, require hydrogen molecules (H_2) to be dissociated into H atoms at a catalytic site. The hydrogen spillover phenomenon was first observed in 1964 in the heterogeneous catalysis system WO_3/Pt [2]. Many subsequent experimental results on hydrogen spillover revealed that H_2 could be easily dissociated on a metal catalyst (although the hydrogen-hydrogen bond in H_2 is strong and therefore unlikely to break under normal reaction conditions), followed by migration of the H atoms to an adjacent support surface (such as reduced metal oxides) and chemisorption there. When considering the optimization of a catalyst, common strategies to achieve the desired activity and selectivity consist in adjusting the crystallographic structure [3-4], particle size [5-10], and geometry of the catalyst [11-14]. Still, synthesizing heterogeneous catalysts with isolated active sites having efficiency at an atomic level with a clarified mechanism remains a critical challenge. Various support materials also affect catalyst optimization significantly. Some examples indicate that strong interactions with the support might enhance the catalytic performance of transition-metal catalysts via charge-transfer effects [15]. Several groups have successfully prepared transition-metal-based single-atom catalysts (SACs) to minimize the amount of metal required to catalyze the hydrogen spillover efficiently, but the catalytic activity still has much room for improvement [16,17].

Since the first report on hydrogen spillover and storage in carbon nanotubes by Dillon et al. [18], carbon supports represent an obvious alternative to metal oxides to exploit hydrogen spillover for storage, even though carbon atoms do not participate directly in the reaction as catalyst, because of their higher inertness relative to conventional oxide supports. Achieving a fundamental understanding of carbon materials as catalyst support is a challenge due to their structural and chemical complexity, which might explain the difficulties in obtaining reproducible adsorption capacities from various studies with volumetric and gravimetric measurements [19,20]. The migration of spillover-dissociated hydrogen atoms is kinetically unfavorable on graphene or graphite [21], which means that hydrogen storage on graphene supports is restricted to small distances around the catalytic sites. How many hydrogen atoms could absorb is thus an important question, which must be addressed for practical applications of H-storage. Inspired by this objective, based on our previous work showing that single Ti atoms adsorb on graphene at the energetically favorite hollow sites [22], and the structural variation upon Ti deposition on graphene and its hydrogen uptake studied by scanning tunneling microscope [23-26], we utilized Ti atomic deposition with a view to mimic SACs on graphene. Unlike previous studies, which used dissociated hydrogen sources (as shown in the Supporting Information Table S1), here we demonstrate that atomically dispersed Ti atoms on crystalline graphene can produce an efficient spillover for hydrogen, which is then chemisorbed

around the anchored Ti SACs. The evaluated H storage capacity exceeds that of Ti nanocluster catalysts at a similar Ti loading.

A well-defined single-crystalline graphene support is suitable as a platform to investigate hydrogen spillover from a single-site Ti catalyst, which dissociates H₂ molecules into H atoms which then migrate to the support graphene (as the receptor of H atoms, schematic illustration in Fig. 1). Hydrogen atoms migrating to the support layer, assisted by the single-site Ti catalyst, can provide substantial storage of atomic hydrogen on graphene in terms of storage quantity. Graphene used in this work was epitaxially grown via thermal decomposition in a resistively heated cold-wall reactor (Aixtron HT-BM) on a hydrogen-etched 4H-SiC (0001) substrate. To achieve a sufficient monolayer uniformity, we grew pristine crystalline graphene in an Ar atmosphere at 1600 K and 780 mbar for 10 min. Single-site catalysts were formed by depositing a sub-monolayer amount of Ti atoms (0.03 to 0.5 ML), calibrated with a quartz crystal microbalance (QCM). The Ti coverage is defined with respect to hexagonal close-packed bulk Ti [23]. Angle-resolved photoemission spectra (ARPES) show a Ti adatom-induced renormalization of the band structure for low Ti coverage (~0.03 ML), as shown in Fig. 2. This was attributed to a strong Ti 3*d* and C 2*p_z* orbital hybridization of isolated Ti-atoms at the graphene hollow sites [22]. After exposing the sample to 4.5 L of H₂ near 300 K (1 L, exposure to 1×10⁻⁶ Torr for 1 s), the significant ARPES spectral contrast in Fig. 2(A) shows a band

gap opening of 280 meV in the graphene. This condition indicates that hydrogen atoms chemisorbed on graphene, which is evidence for the dissociation of gaseous H₂ molecules and hydrogen spillover by isolated Ti SACs. Moreover, without Ti, neither band structure modification nor renormalization was observed in the ARPES spectrum of graphene after H₂ exposure, as shown in Supporting Information Fig. S1. Thus, the Ti catalysis facilitates the dissociation of molecular H₂ and the hydrogenation of graphene near 300 K in vacuum.

To quantitatively understand the spillover effect on graphene, we monitored the band gaps of graphene before and after exposure to H₂ using energy-dispersion curves (EDC) extracted from ARPES (insets of Fig. 2 (B)). Calculations [27-29] yielded valuable information on the origin of the graphene band-structure modulations induced by C–H bonds, from fully hydrogenated insulating graphene sheets to partially hydrogenated graphene displaying semiconducting properties, with band gaps depending on the H coverage of graphene. The band gap value can thus serve to quantify the number of hydrogen atoms incorporated in partially hydrogenated graphene. Based on the DFT-based theoretical results shown in Fig. 2(B) [27-29], a quadratic relation $\Delta E_g = A_2 \eta^2 + A_1 \eta + A_0$ is obtained. η is the absorbed hydrogen coverage on graphene (H/C value, i.e., the H storage capacity of graphene), $A_2 = 2.49$ eV, $A_1 = 1.47$ eV, and $A_0 = 9.67 \times 10^{-2}$ eV. The band-gap opening (ΔE_g) increases from about 0 to 1.5 eV as η increases from 0 to 50 %. The H-storage capacity η of

partially hydrogenated graphene with band gap 280 meV is estimated to be about 10.6 % (0.88 wt%).

As indicated in Fig. 2(B), this value is in between a lower limit of 7.3 % (0.6 wt%) obtained with the DFT+PBE approach and an upper limit of 16.2 % (1.33 wt%) with the DFT+GGA approach [27-29].

Previous theoretical and experimental work clearly showed that charge transfer between the catalyst and the support generates a noticeable impact on the electrocatalytic activity of the catalyst [30,31].

As we have concluded in our previous work [22], the anchored Ti SACs contributes a pronounced electron transfer from Ti to the graphene support ($0.45 e^-$ per Ti atom), which leads to an n-type doping of graphene. Thus, we attribute the high storage activity observed here to the charge transfer between Ti atoms and graphene, which provides a more efficient and safer method for using SACs on graphene.

To explore the nature of the formation of C–H bonds accompanying hydrogenation, we recorded X-ray absorption spectroscopy (XAS) data on Ti-decorated graphene after exposure to H_2 , following the same sample preparation procedure as for the ARPES experiment. We recorded the XAS at an X-ray beam incident angle of 0° relative to the surface normal. The C–H* resonance region is presented in Figure 3, for Ti-doped (~ 0.03 ML) and H_2 -dosed (~ 4.5 and 49.5 L) samples. We plot the spectral differences, i.e. spectra from which the spectrum of pristine graphene is subtracted. A prominent spectral feature is clearly visible centered at 287.5 eV, which is attributed to the C–H* resonance

[32,33]. Its intensity increases significantly after H₂ dosage, while the Ti-decorated graphene (without hydrogen dosing) shows no sign of C–H bonds. This result clearly indicates the formation of C–H bond after exposing the Ti SAC-loaded graphene to hydrogen, implying the spillover of hydrogen onto the graphene support. The full-range carbon *K*-edge spectra are shown in the Supporting Information Section 4.

To seek the optimal H storage capacity, we recorded *in situ* ambient pressure X-ray photoemission spectra (APXPS) with a larger amount of Ti catalyst loading and under a larger H₂ exposure (1 mbar), to monitor the C–H bonding structure including the underlying substrate. This is useful to clarify their roles in the progressively hydrogenated Ti-decorated graphene under a nearly ambient gaseous pressure. Figure 4 shows the synchrotron-radiation excited C 1s core-level spectra recorded *in situ* near 300 K taken from pristine graphene, Ti-deposited graphene (Ti ~ 0.5 ML), and Ti-deposited graphene under H₂ exposure for one hour (Ti + H₂). By analyzing the measured C 1s core-level spectra with a Doniach-Sunjić line shape and comparing them to reference spectra of non-hydrogenated crystalline graphene grown on a SiC substrate, both measured here and from literature, the amount of hydrogen stored in our graphene samples can be precisely determined. Details of the fitting results of the C 1s APXPS spectra are listed in Table S3 in the Supporting Information Section 6. The C 1s core-level spectra of pristine and Ti-deposited graphene are well fitted with one graphene

sp^3 bonding peak (Gr at 284.4 eV), one SiC bulk component peak (B at 283.3 eV), and two interfacial components S1 and S2 related to localized reconstruction bonds, they represent a $(6\sqrt{3} \times 6\sqrt{3})R30^\circ$ reconstructed SiC(0001) surface formed underneath the epitaxial graphene as a buffer layer [34]. A Shirley background was included in the fitting procedure. The interfacial state S1 at 284.2 eV can be identified with the covalent bonding between the buffer layer and SiC substrate, and S2 at 285.0 eV is due to the sp^2 -bonded C atoms within the buffer layer. These two interfacial states S1 and S2 have a constant area ratio of $\sim 1/2$ [34,35]. They would not be affected by covering the sample with Ti catalysts and H atoms, which is consistent with the XPS results of epitaxial graphene on SiC (0001) substrate [35-37]. With Ti deposition and hydrogenation, the C 1s core level shows a progressive attenuation due to the Ti metal covering and chemisorption of atomic hydrogen. Hydrogen bonding to graphene implies that the H atom induces an out-of-plane C–H bond (Gr1, hydrogenated C atom) and can be detected in the C 1s spectrum at a higher binding energy position of 285.0 eV than sp^2 graphene (G) at 284.4 eV, which is consistent with the previous result of hydrogen adsorption in graphene [38]. Furthermore, another component appears in the spectrum (Gr2), which is due to non-hydrogenated C atoms adjacent to C–H bonds, as illustrated in Fig. 4. Therefore, the line shape of Gr changes gradually upon hydrogenation, and two shoulder peaks appear with respect to Gr, which are 0.6 eV higher (Gr1) and 0.2 eV lower (Gr2) in binding energy [39-42]. Thus, the Gr1 peak area is

highly reliable for quantitative determination of the hydrogen content, using $\eta(\%) = \text{Gr1}/(\text{Gr}+\text{Gr1}+\text{Gr2})$. We found here hydrogenated graphene with a H coverage of about $\eta \sim 13.5 \pm 0.5 \%$ (or $1.11 \pm 0.04 \text{ wt}\%$), which is larger than previous reports about atomic hydrogenation of crystalline graphene ($\eta \sim 8.7$ to 9%) [41,43].

The hydrogen storage by spillover is a process of adsorption of atomic hydrogen, in which the numbers of catalytic sites and H adsorption sites determine the storage capacity. The density of SAC active sites, i.e., the hollow sites occupied by Ti atoms, were estimated based on the Ti coverage of 0.03 ML, which corresponds to $4.0 \times 10^{13} \text{ cm}^{-2}$ for the Ti SAC density. How far H atoms can migrate from the Ti catalyst is dominated by the macroscopic diffusion coefficient (L_D). According to a 2D-random-walk model for diffusion, L_D can be expressed with a potential diagram in the classical limit. The diffusion length of H on graphene was estimated with this equation,

$$L_D = (D_0 \tau_0)^{0.5} \exp\left(\frac{E_{ad}-E_{dif}}{2k_B T}\right) \quad (1)$$

in which E_{ad} and E_{dif} are the adsorption and diffusion energies of H on graphene, which are 78 KJ/mol and 91KJ/mol, respectively [44]. D_0 and τ_0 are the pre-exponential factors of diffusion and residence period of C–H bonds on graphene. Their values are $3276 \text{ \AA}^2/\text{ps}$ and 1.52 ps, respectively [45]. Near 300 K, the diffusion length L_D is thus about 2.7 \AA , which is only twice the C–C bond length, $a = 1.42 \text{ \AA}$. As the Ti catalyst atoms are anchored on the energetically favorable graphene hollow sites,

the spillover H atoms diffuse isotropically and are restricted to small distances around the Ti catalytic center on the graphene surface, as depicted in Fig. 5 (A). This schematic illustration reveals that graphene hydrogenation occurs only on the first nearest-neighbor sublattices (i.e. one Ti surrounded by six H atoms). As shown in Supporting Information Section 5, the H-storage capacity η of Ti SACs with an amount 0.03 ML is estimated to be about 6.3 %. This value is closed to the low limit value ($\eta \sim 7.3$ %) extracted from the partially hydrogenated graphene band gap and near that of most metal catalysts on various carbon supports, especially the reported atomic metal species on carbon supports under high pressure [20,46,47].

Furthermore, when the deposition of Ti reaches 0.5 ML, H-storage capacity η increased non-linearly to 13.5 % according to the APXPS result. This indicates that for Ti deposition above 0.1 ML, the single Ti atoms are generally susceptible to aggregate to become nanoclusters on graphene, consistent with previous STM studies [23]. For Ti nanoclusters adopting a hexagonal close-packed cluster configuration (for details, see Supporting Information Section 5) [48], the number of C–H bonding sites can be estimated to be within a concentric circular area from the nanocluster boundary to an outer diameter, which is larger by L_D . This is shown in Fig. 5 (A) for the case of a Ti nanocluster with Ti atom number $N=10$. With increasing Ti coverage on graphene, the number of H atoms stored around each Ti nanocluster increases sub-linearly, while the H-storage performance per Ti atom

decreases sharply, as shown in Fig. 5 (B) (see also Supporting Information Table S2). Thus, due to the coalescence of Ti atoms into larger nanoclusters, the hydrogen storage capacity η does not increase linearly with the Ti catalyst loading on graphene. Furthermore, to boost η to 100 % on graphene, the full utilization of Ti SACs on graphene (6.3×10^{14} sites cm^{-2} for 0.48 ML) with a Ti_1H_6 structure would need to form, as illustrated in Fig. 5 (C). Even though the H-storage capacity at ambient temperature and in vacuum reported here is still below the DOE onboard vehicular target (~ 7.5 wt%), simultaneously enhancing the number of Ti SACs on graphene and high-pressure H_2 loading is anticipated to increase the performance for practical onboard hydrogen storage for vehicular fuel cells. Also, the H-storage capacity shown here is significantly larger than all reported results of high-pressure hydrogen-storage measurements on carbon nanotubes, graphene, and Pt-decorated graphene [1,20,46,47].

In conclusion, we designed and implemented hydrogen spillover from single-atom to single-cluster catalysts by precisely controlling the Ti coverage on graphene. The atomic nature of C–H bonds on graphene and the optimal amount of H storage capacity were spectrally characterized with ARPES and XAS. Our photoemission data were quantitatively explained by a short migration distance of H atoms diffusing at room temperature on graphene. Our finding provides a general rule

that will enable a rational design of carbon-supported physisorbed metal catalysts for chemisorbed H-storage via spillover.

Supporting Information

This material is available free of charge via the internet at <http://pubs.acs.org>.

Details of experimental methods, crystal growth, and additional experimental results and discussion.

Acknowledgements

We thank Dr. Yeu-Kuang Hwu of Academia Sinica for providing a mu-metal chamber for the ARPES measurements and NSRRC beamline staff for skillful assistance during SR experiments. This work was funded by Taiwan Ministry of Science and Technology.

References

1. Bhowmick, R.; Rajasekaran, S.; Friebel, D.; Beasley, C.; Jiao, L.; Ogasawara, H.; Dai, H.; Clemens, B. and Nilsson, A. Hydrogen Spillover in Pt-Single-Walled Carbon Nanotube Composites: Formation of Stable C–H Bonds. *J. Am. Chem. Soc.* **133**, 14, 5580 (2011)
2. Khoobiar, S. Particle to Particle Migration of Hydrogen Atoms on Platinum-Alumina Catalysts from Particle to Neighboring Particles. *J. Phys. Chem. C* 1964 **68**, 411 (1964)
3. Fu, Q.; Li, W.-X.; Yao, Y.; Liu, H.; Su, H.-Y.; Ma, D.; Gu, X.-K; Chen, L.; Wang, Z.; Zhang, H.; Wang, B. and Bao, X. Interface-Confined Ferrous Centers for Catalytic Oxidation. *Science* **328**, 1141 (2010)
4. Nunez, M.; Lansford, J. L. and Vlachos, D. G. Optimization of the facet structure of transition-metal catalysts applied to the oxygen reduction reaction. *Nature Chemistry* **11**, 449 (2019)
5. Yang, X.-F.; Wang, A.; Qiao, B.; Li, J.; Liu J. and Zhang, T. Single-Atom Catalysts: A New Frontier in Heterogeneous Catalysis. *Acc. Chem. Res.* 2013 **46**, 1740-1748.
6. Turner, M.; Golovko, V. B.; Vaughan, O. P. H.; Abdulkin, P.; Berenguer, A.; Tikhov, M. S.; Johnson, B. F. G. and Lambert, R. M. Selective oxidation with dioxygen by gold nanoparticle catalysts derived from 55-atom clusters. *Nature* **454**, 981 (2008)
7. Lei, Y.; Mehmood, F.; Lee, S.; Greeley, J.; Lee, B.; Seifert, S.; Winans, R. E.; Elam, J. W.; Meyer,

- R. J.; Redfern, P. C.; Teschner, D.; Schlogl, R.; Pellin, M. J.; Curtiss, L. A. and Vajda S. Increased silver activity for direct propylene epoxidation via subnanometer size effects. *Science* **328**, 224 (2010)
8. Qiao, B.; Wang, A.; Li, L.; Lin, Q.; Wei, H.; Liu, J. and Zhang, T. Ferric Oxide-Supported Pt Subnano Clusters for Preferential Oxidation of CO in H₂-Rich Gas at Room Temperature. *ACS Catal.* **4**, 2113 (2014)
9. Qiao, B.; Wang, A.; Yang, X.; Allard, L. F.; Jiang, Z.; Cui, Y.; Liu, J.; Li, J. and Zhang, T. Single-atom catalysis of CO oxidation using Pt₁/FeO_x. *Nature Chemistry* **3**, 634 (2011)
10. Tsunoyama, H.; Sakurai, H.; Negishi, Y. and Tsukuda, T. Size-specific catalytic activity of polymer-stabilized gold nanoclusters for aerobic alcohol oxidation in water. *J. Am. Chem. Soc.* **127**, 9374 (2005)
11. Wang, X.; Liu, Y.; Zhang, T.; Luo, Y.; Lan, Z.; Zhang, K.; Zuo, J.; Jiang, L. and Wang, R. Geometrical-Site-Dependent Catalytic Activity of Ordered Mesoporous Co-Based Spinel for Benzene Oxidation: In Situ DRIFTS Study Coupled with Raman and XAFS Spectroscopy. *ACS Catal.* **7**, 1626 (2017)
12. Li, J.; Huang, G.; Ye, M.; Li, M.; Liu, R. and Mei, Y. Dynamics of catalytic tubular microjet engines: Dependence on geometry and chemical environment. *Nanoscale* **3**, 5083 (2011)

13. Nørskov, J. K.; Bligaard, T.; Hvolbaek, B.; Abild-Pedersen, F.; Chorkendorff, I. and Christensen, C. H. The nature of the active site in heterogeneous metal catalysis. *Chem. Soc. Rev.* **37**, 2163 (2008)
14. Zhao, S.; Chen, F.; Duan, S.; Shao, B.; Li, T.; Tang, H.; Lin, Q.; Zhang, J.; Li, L.; Huang, J.; Bion, N.; Liu, W.; Sun, H.; Wang, A.-Q.; Haruta, M.; Qiao, B.; Li, J.; Liu, J. and Zhang, T. Remarkable active-site dependent H₂O promoting effect in CO oxidation. *Nature Communications* **10**, 3824 (2019)
15. Kumar, G.; Tibbitts, L.; Newell, J.; Panthi, B.; Mukhopadhyay, A.; Rioux, R. M.; Pursell, C. J.; Janik, M. and Chandler, B. D. Evaluating differences in the active-site electronics of supported Au nanoparticle catalysts using Hammett and DFT studies. *Nat. Chem.* **10**, 268 (2018)
16. Lin, J.; Wang, A.; Qiao, B.; Liu, X.; Yang, X.; Wang, X.; Liang, J.; Li, J.; Liu, J. and T. Zhang, T. Remarkable Performance of Ir₁/FeO_x Single-Atom Catalyst in Water Gas Shift Reaction. *J. Am. Chem. Soc.* **135**, 15314 (2013)
17. Liang, J.-X.; Lin, J.; Yang, X.-F.; Wang, A.-Q.; Qiao, B.-T.; Liu, J.; Zhang, T. ; Li, J. Theoretical and Experimental Investigations on Single-Atom Catalysis: Ir₁/FeO_x for CO Oxidation. *J. Phys. Chem. C* **118**, 21945 (2014)
18. Dillon, A. C.; Jones, K. M.; Bekkedahl, T. A.; Kiang, C. H.; Bethune, D. S. and Heben, M. J.

Storage of hydrogen in single-walled carbon nanotubes. *Nature* **386**, 377 (1997)

19. Yurum, Y.; Taralp, A. and Veziroglu, T. N. Storage of hydrogen in nanostructured carbon materials. *Int. J. Hydrogen Energy* **34**, 3784 (2009)
20. Srinivas, G.; Zhu, Y.; Piner, R.; Skipper, N.; Ellerby, M. and Ruoff, R. Synthesis of graphene-like nanosheets and their hydrogen adsorption capacity. *Carbon* **48**, 630 (2010)
21. Prins, R. Hydrogen spillover. Facts and fiction. *Chem. Rev.* **112**, 2714 (2012)
22. Chen, J. W.; Huang, H. C.; Convertino, D.; Coletti, C.; Chang, L. Y.; Shiu, H. W.; Cheng, C. M.; Lin, M. F.; Heun, Stefan; Chien, Forest S. S.; Chen, Y. C.; Chen, C. H. and Wu, C. L. Efficient n-type doping in epitaxial graphene through strong lateral orbital hybridization of Ti adsorbate. *Carbon* **109**, 300 (2016)
23. Mashoff, T.; Takamura, M.; Tanabe, S.; Hibino, H.; Beltram, F. and Heun, S. Hydrogen storage with titanium-functionalized graphene. *Appl. Phys. Lett.* **103**, 013903 (2013)
24. Mashoff, T.; Convertino, D.; Miseikis, V.; Coletti, C.; Piazza, V.; Tozzini, V.; Beltram, F. and Heun, S. Increasing the active surface of titanium islands on graphene by nitrogen sputtering. *Appl. Phys. Lett.* **106**, 083901 (2015)
25. Takahashi, K.; Isobe, S.; Omori, K.; Mashoff, T.; Convertino, D.; Miseikis, V.; Coletti, C.; Tozzini, V. and Heun, S. Revealing the multibonding state between hydrogen and graphene-

- supported Ti clusters. *J. Phys. Chem. C*, **120**, 12974 (2016)
26. Murata, Y.; Veronesi, S.; Whang, D. and Heun, S. Morphology of Ti on Monolayer Nanocrystalline Graphene and Its Unexpectedly Low Hydrogen Adsorption. *J. Phys. Chem. C*, **123**, 1572 (2019)
27. Li, M.; Wang, L.; Yu, N.; Sun, X.; Hou, T. and Li, Y. Structural stability and band gap tunability of single-side hydrogenated graphene from first-principles calculations. *J. Mater. Chem. C*, **3**, 3645 (2015)
28. Wang, X.; Zhang, G.; Wang, Z.; Yang, L.; Li, X.; Jiang, J. and Luo, Y. Metal-enhanced hydrogenation of graphene with atomic pattern. *Carbon* **143**, 700 (2019)
29. Balog, R.; Jorgensen, B.; Nilsson, L.; Andersen, M.; Rienks, E.; Bianchi, M.; Fanetti, M.; Laegsgaard, E.; Baraldi, A.; Lizzit, S.; Sljivancanin, Z.; Besenbacher, F.; Hammer, B.; Pedersen, T. G.; Hoffmann, P. and Hornekaer, L. Bandgap opening in graphene induced by patterned hydrogen adsorption. *Nat. Mater.* **9**, 315 (2010)
30. Gerber, I. C. and Serp, P. A theory/experience description of support effects in carbon-supported catalysts. *Chemical Reviews* **120**, 1250 (2020)
31. Wood, K. N.; O'Hayre, R. and Pylypenko, S. Recent progress on nitrogen/carbon structures designed for use in energy and sustainability applications. *Energy Environ. Sci.* **7**, 1212 (2014)

32. Ade, H. and Stoll, H. Near-edge X-ray absorption fine-structure microscopy of organic and magnetic materials. *Nature Materials*, **8**, 281 (2009)
33. Feng, X.; Song, M.; Stolte, W. C.; Gardenghi, D.; Zhang, D.; Sun, X.; Zhu, J.; Cairns, E. J. and Guo, J. Understanding the degradation mechanism of rechargeable lithium/sulfur cells: a comprehensive study of the sulfur–graphene oxide cathode after discharge–charge cycling. *Phys. Chem. Chem. Phys.*, **16**, 16931 (2014)
34. Riedl, C.; Coletti, C.; Iwasaki, T.; Zakharov, A. A. and Starke, U. Quasi-free-standing epitaxial graphene on SiC obtained by hydrogen intercalation. *Phys. Rev. Lett.* **103**, 246804 (2009)
35. Schumann, T.; Dubsclaff, M.; Oliveira Jr, M. H.; Hanke, M.; Fromm, F.; Seyller, T.; Nemeč, L.; Blum, V.; Scheffler, M.; Lopes, J. M. J. and Riechert H. Structural investigation of nanocrystalline graphene grown on $(\sqrt{3} \times \sqrt{3})R30$ -reconstructed SiC surfaces by molecular beam epitaxy. *New J. Phys.* **15**, 123034 (2013)
36. Emtsev, K. V.; Speck, F.; Seyller, T.; Ley, L. and Riley, J. D. Interaction, growth, and ordering of epitaxial graphene on SiC {0001} surfaces: A comparative photoelectron spectroscopy study. *Phys. Rev. B* **77**, 155303 (2008)
37. Jørgensen, J. H.; Cabo, A. G.; Balog, R.; Kyhl, L.; Groves, M. N.; Cassidy, A. M.; Bruix, A.; Bianchi, M.; Dendzik, M.; Arman, M. A.; Lammich, L.; Pascual, J. I.; Knudsen, J.; Hammer,

- B.; Hoffmann, P. and Hornekaer, L. Symmetry-driven band gap engineering in hydrogen functionalized graphene. *ACS Nano* **10**, 10798 (2016)
38. Rajasekaran, S.; Abild-Pedersen, F.; Ogasawara, H.; Nilsson, A.; and Kaya, S. Interlayer carbon bond formation induced by hydrogen adsorption in few-layer supported graphene. *Phys. Rev. Lett.* **111**, 085503 (2013)
39. Nikitin, A.; Ogasawara, H.; Mann, D.; Denecke, R.; Zhang, Z.; Dai, H.; Cho, K. and Nilsson, A. Hydrogenation of single-walled carbon nanotubes. *Phys. Rev. Lett.* **95**, 225507 (2005)
40. Haberer, D.; Vyalikh, D. V.; Taioli, S.; Dora, B.; Farjam, M.; Fink, J.; Marchenko, D.; Pichler, T.; Ziegler, K.; Simonucci, S.; Dresselhaus, M. S.; Knupfer, M.; Buchner, B.; and Gruneis, A. Tunable band gap in hydrogenated quasi-free-standing graphene. *Nano Lett.* **10**, 3360 (2010)
41. Nikitin, A.; Näslund, L.; Zhang, Z.; and Nilsson, A. C–H bond formation at the graphite surface studied with core level spectroscopy. *Surf. Sci.* **602**, 2575 (2008)
42. Riedl, C.; Coletti, C. and Starke, U. Structural and electronic properties of epitaxial graphene on SiC (0001): a review of growth, characterization, transfer doping and hydrogen intercalation. *J. Phys. D: Appl. Phys.* **43**, 374009 (2010)
43. Haberer, D.; Giusca, C. E.; Wang, Y.; Sachdev, H.; Fedorov, A. V.; Farjam, M.; Jafari, S. A.; Vyalikh, D. V.; Usachov, D.; Liu, X.; Treske, U.; Grobosch, M.; Vilkov, O.; Adamchuk, V. K.;

- Irle, S.; Silva, S. R. P.; Knupfer, M.; Büchner, B.; Grüneis, A. Evidence for a New Two-Dimensional C₄H-Type Polymer Based on Hydrogenated Graphene. *Adv. Mater.* **23**, 4497 (2011)
44. Ferro, Y.; Marinelli, F.; Jelea A.; Allouche, A. Adsorption, diffusion, and recombination of hydrogen on pure and boron-doped graphite surfaces. *J. Chem. Phys.* **120**, 11882 (2004)
45. Herrero, C. P. and Ramirez, R. Diffusion of hydrogen in graphite: a molecular dynamics simulation. *J. Phys. D: Appl. Phys.* **43**, 255402 (2010)
46. Bacsa, R.; Laurent, C.; Morishima, R.; Suzuki, H. and Lay, M. L. Hydrogen storage in high surface area carbon nanotubes produced by catalytic chemical vapor deposition. *J. Phys. Chem. B* **108**, 12718 (2004)
47. Ma, L. P.; Wu, Z. S.; Li, J.; Wu, E. D.; Ren, W. C. and Cheng, H. M. Hydrogen adsorption behavior of graphene above critical temperature. *Int. J. Hydrogen Energy* **34**, 2329 (2009)
48. Kaatz, F. H. and Bultheel, A. Magic mathematical relationships for nanoclusters. *Nanoscale Res. Lett.* **14**, 150 (2019)

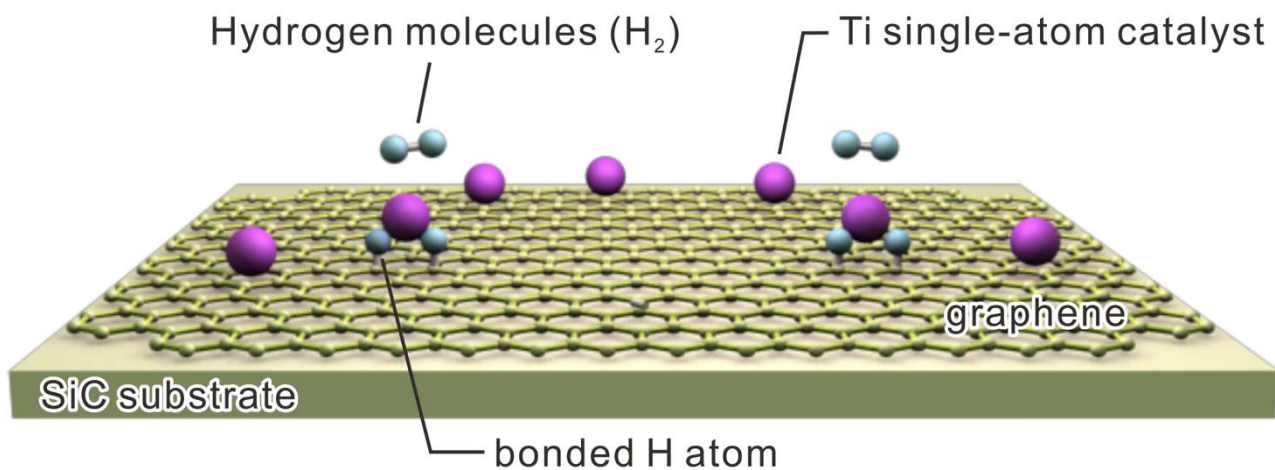


FIG. 1 (color). Schematic diagram of the spillover effect of Ti on graphene, which involves dissociation of molecular hydrogen near 300 K, migration of hydrogen atoms on epitaxial graphene and their chemisorption.

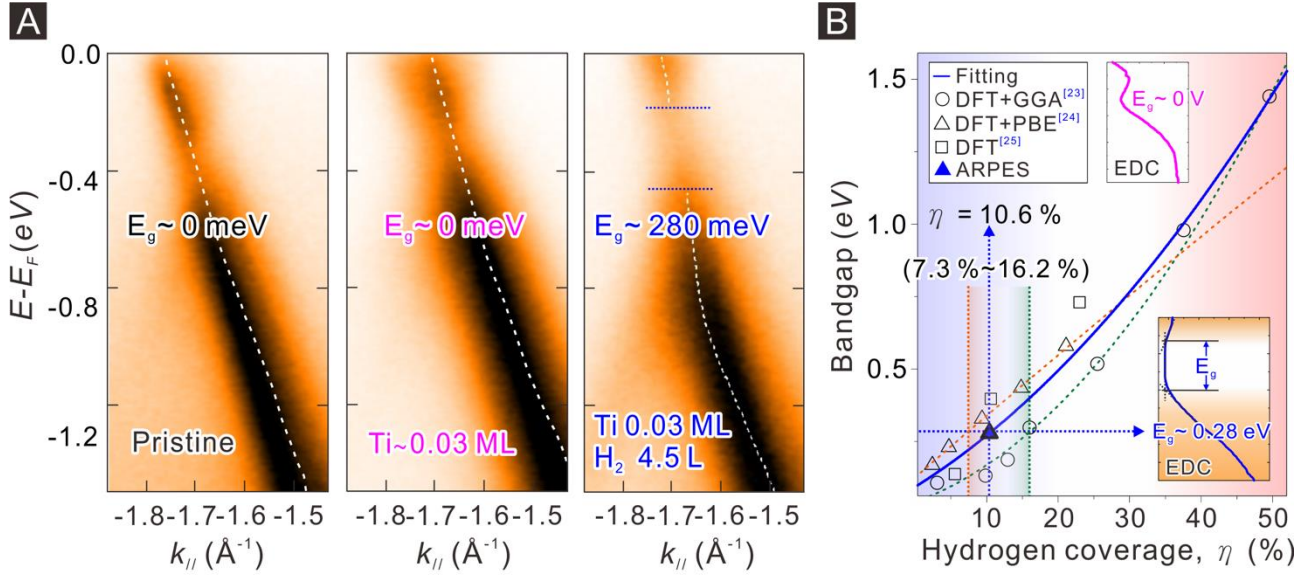


FIG. 2 (color). ARPES measurements performed on pristine epitaxial graphene, after Ti deposition, and after a subsequent dose of H₂ molecules (H₂ = 4.5 L) near 300 K. (A) Band structure of pristine and Ti-doped graphene for 0.03 ML. The sample was then exposed to a 4.5 L dose of H₂. The data were taken along direction K→ Γ in the vicinity of the K-point. White dashed lines indicate the energy dispersion fitted by the momentum dispersion curves (MDC). (B) Data points from previously performed DFT calculations [27,28,29] were used to obtain the extent of graphene hydrogenation from the measured band gap induced by H-C bonds. The dependence of the bandgap of graphene on H coverage is $\Delta E_g = A_2 \eta^2 + A_1 \eta + A_0$, with $\eta = H/C$, $A_2 = 2.49 \text{ eV}$, $A_1 = 1.47 \text{ eV}$, and $A_0 = 9.67 \times 10^{-2} \text{ eV}$. The hydrogen coverage η corresponding to graphene band gap $E_g = 0.28 \text{ eV}$ is obtained via two different approaches, with a lower limit of 7.3 % and an upper limit of 16.2 % using a fit of DFT+PBE and DFT+GGA data, respectively. Insets show angle-integrated curves of energy distribution (EDC) in the vicinity of the K point taken before (red) and after (blue) 4.5 L H₂ dosage for graphene with 0.03 ML Ti.

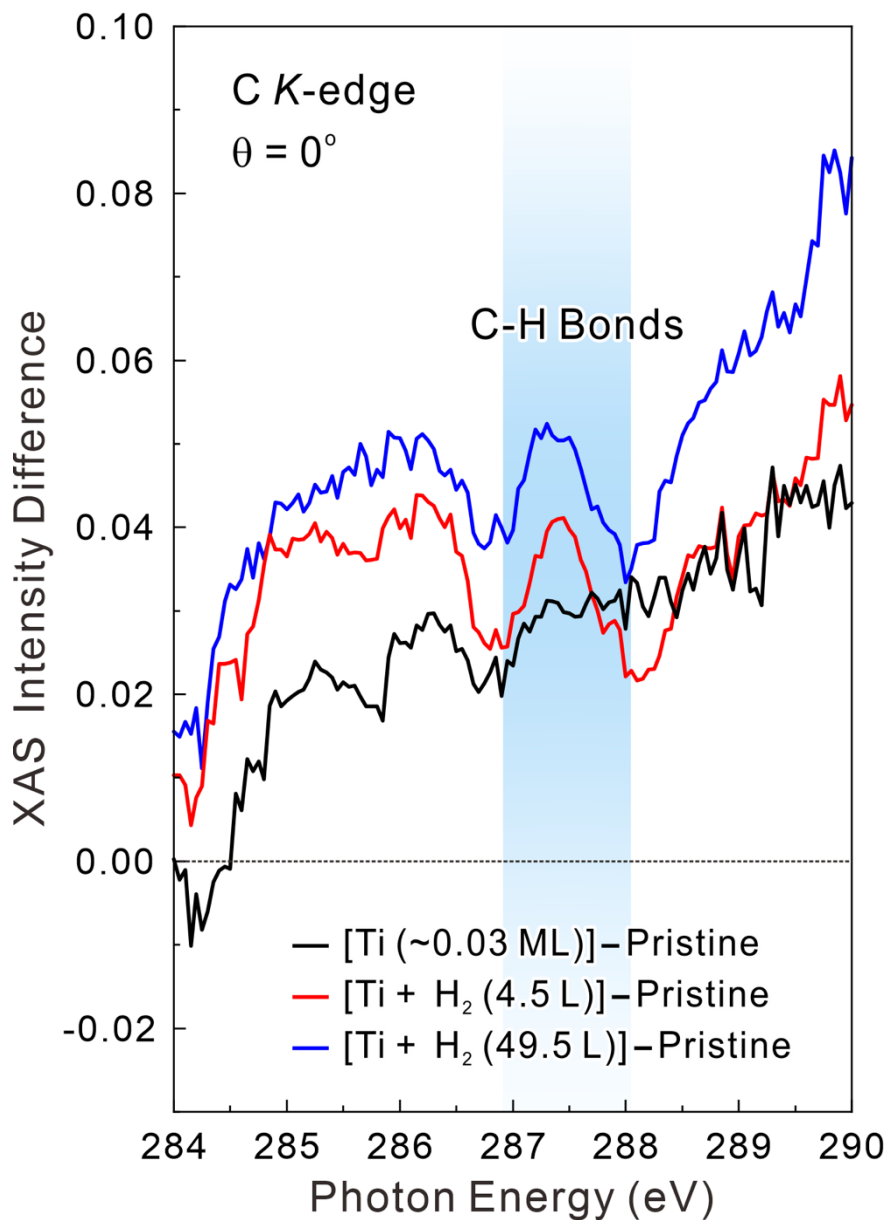


FIG. 3 (color). C–H* resonance region of the Carbon *K*-edge X-ray absorption spectra for Ti-doped (black curve), for 4.5 L H₂-dosed (red curve), and for 49.5 L H₂-dosed (blue curve) samples. We show difference spectra, i.e., spectra minus the spectrum of pristine graphene. The shaded area indicates the position of the C–H* resonance. See Supporting Information Section 3 for full spectra.

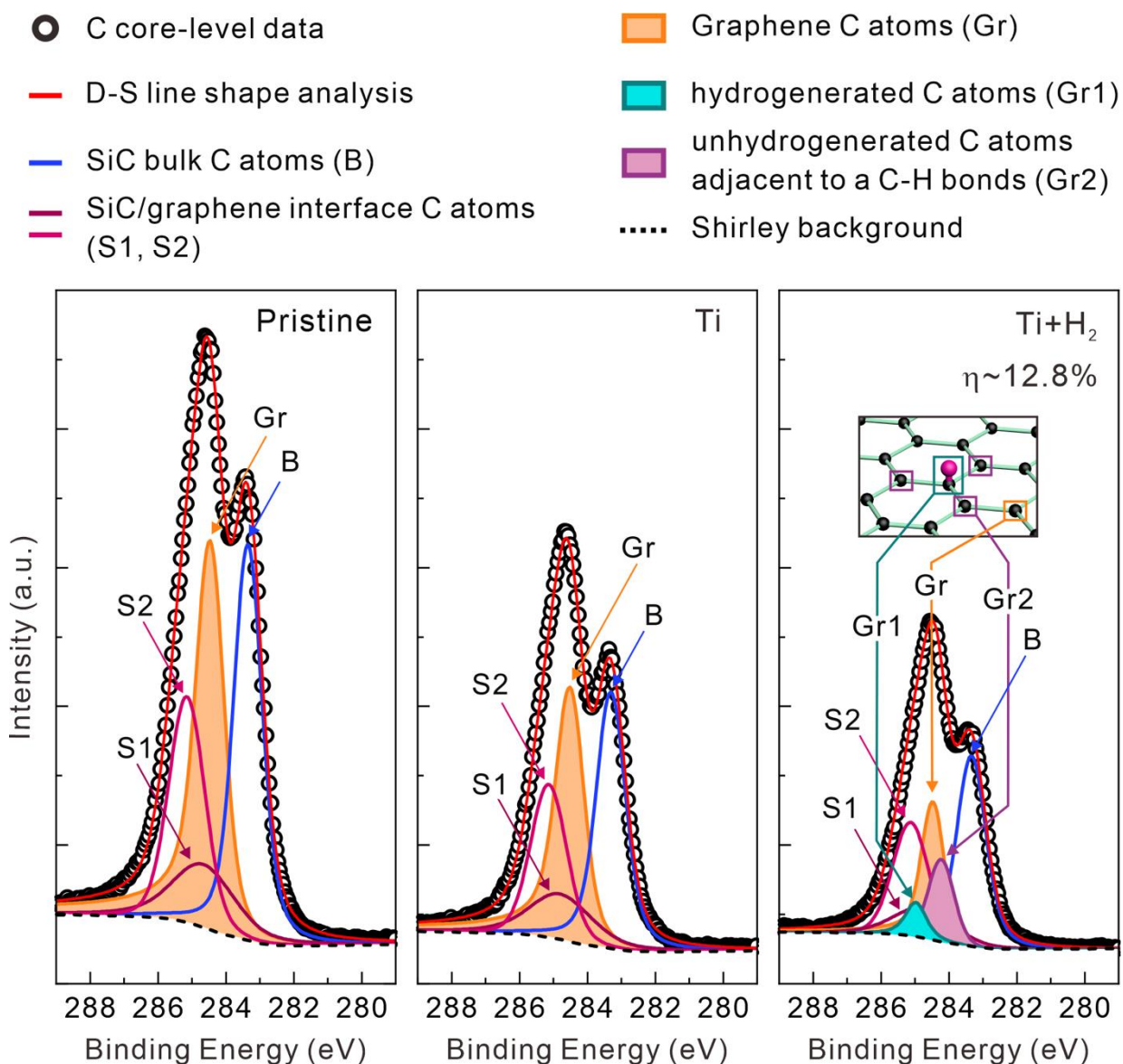


FIG. 4 (color). From left to right: APXPS C 1s spectra of pristine, Ti-deposited (0.5 ML), and Ti + H₂ exposed graphene (H₂ 1 mbar for 1 hour). Spectra were deconvoluted using Gaussian-broadened Doniach-Sunjc (DS) functions including Shirley background. Gr, B, and S1, S2 indicate C 1s chemical environments for graphene, SiC bulk, and interfacial reconstruction (at the buffer layer interface), respectively. Component Gr1 represents hydrogenated C atoms (C–H bond) of graphene. Gr2 represents not-hydrogenated C atoms next to C–H bonds, as illustrated in the inset. From the integrated area of the relative constituents of the graphene C 1s C–H components (Gr, Gr1, Gr2), we estimate $\eta \sim 13.5\%$ hydrogen coverage.

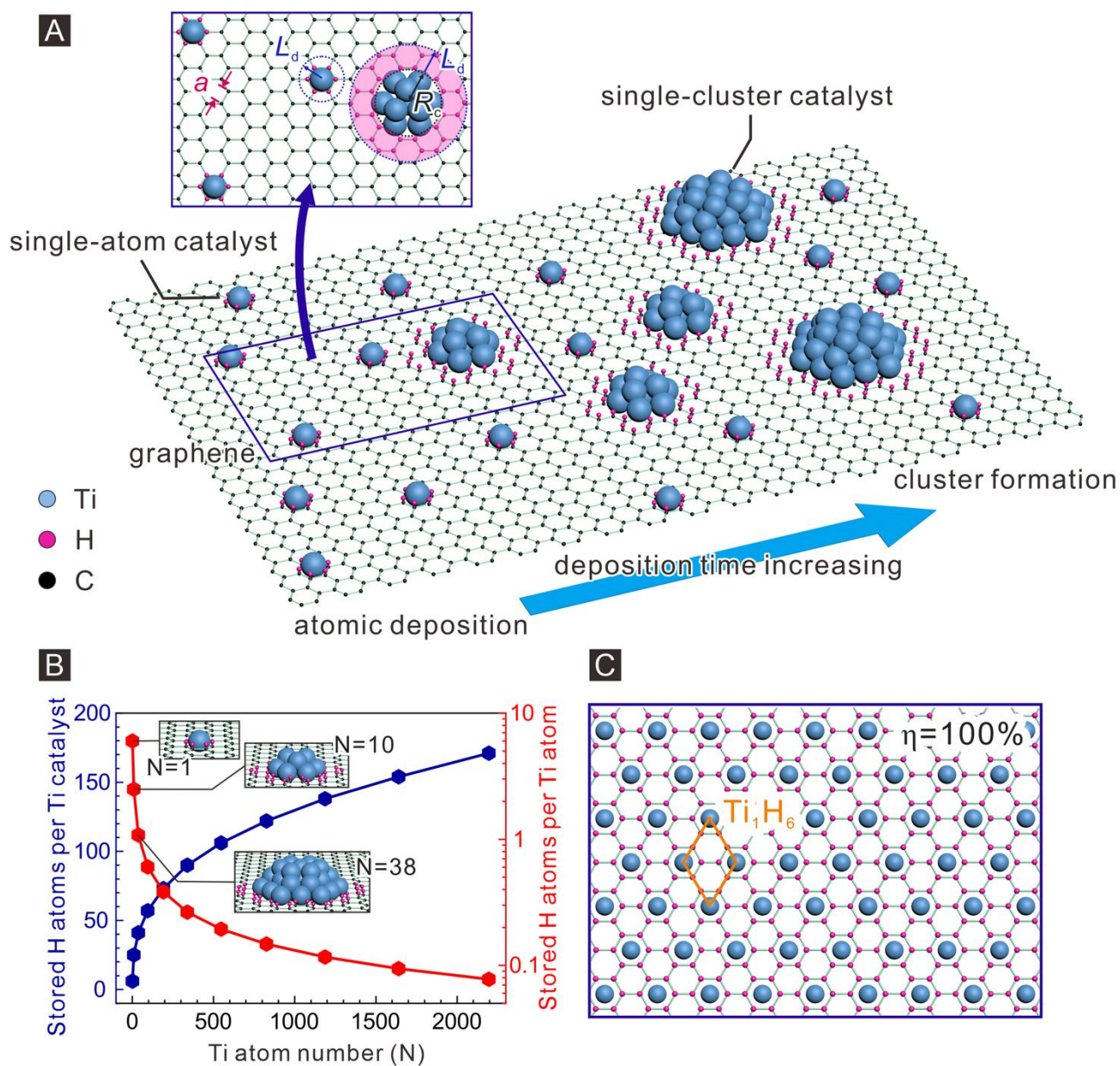
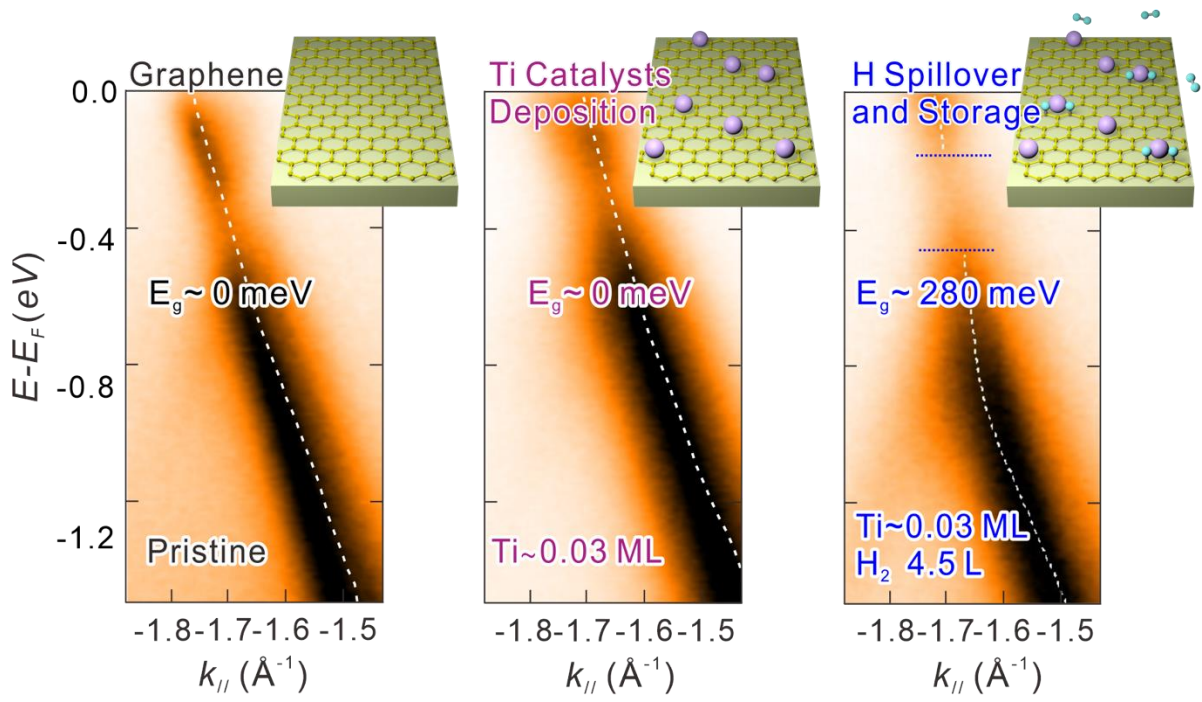


FIG. 5 (color). (A) Schematic diagram of single-atom to single-cluster catalyst formation. Low to high Ti deposition was explored to obtain well-isolated atoms or nanocluster catalysts on graphene. From the spillover of H atoms for an isolated Ti atom and Ti nanocluster catalyst, the 2D-diffusion length (L_D) and nanocluster size (diameter R_C) can be used to estimate the H-storage capacity for small and large Ti coverages. (B) Calculated H storage of Ti SACs and Ti nanoclusters with truncated bipyramid shape versus number N of Ti atoms. (C) Schematic illustration of full H storage ($\eta=100\%$) on graphene with the help of Ti SACs through the formation of a Ti_1H_6 structure.

ToC Figure:



Supporting Information for

Hydrogen spillover and storage on graphene with single-site Ti catalysts

Jih-Wei Chen^{1,2}, Shang-Hsien Hsieh², Sheng-Shong Wong¹, Ya-Chi Chiu¹, Hung-Wei Shiu², Chia-Hsin Wang², Yaw-Wen Yang², Yao-Jane Hsu², Domenica Convertino³, Camilla Coletti³, Stefan Heun⁴, Chia-Hao Chen^{2*}, and Chung-Lin Wu^{1,2*}

¹Department of Physics, National Cheng Kung University, Tainan 70101, Taiwan

²National Synchrotron Radiation Research Center, Hsinchu 30076, Taiwan

³Center for Nanotechnology Innovation @ NEST, Istituto Italiano di Tecnologia, Pisa 56127, Italy

⁴NEST, Istituto Nanoscienze-CNR and Scuola Normale Superiore, 56127 Pisa, Italy

1. Experimental methods

Crystal growth

Graphene was grown via thermal decomposition in a resistively heated cold-wall reactor (Aixtron HT-BM) on a hydrogen-etched 4H-SiC (0001) substrate. The growth was performed under Ar atmosphere, at 1600 K and 780 mbar for 10 min. The quality and homogeneity of the monolayer graphene was assessed with a combined analysis of Raman spectra and atomic-force microscopy. Before ARPES, XAS, and APXPS measurements, the graphene samples were annealed at 900 K for more than 7 h under UHV conditions.

Details of measurements

ARPES was used to probe the electronic structure of pristine graphene and of Ti-decorated graphene, with and without the dosage of H₂ molecules. APXPS measurements were performed to determine the percentage of hydrogenation of Ti-decorated graphene as H₂ molecules adsorbed. After dosing the sample under continuous flow of H₂ for various time periods, the ARPES and APXPS data were measured after the chamber was pumped down to the base pressure. Analyzers (SPECS Phoibos 150 and SPECS Phoibos 150 NAP) were utilized to measure the ARPES and APXPS spectra, respectively. Measurements were performed at Taiwan Light Source (TLS) beamlines 08A1 and 24A1 of the National Synchrotron Radiation Research Center (NSRRC) in Hsinchu, Taiwan. All measurements were performed near 300 K. Energy and momentum resolution are estimated to be better than 150 meV and $\pm 0.005 \text{ \AA}^{-1}$ for ARPES. Energy resolution is estimated to be better than 280 meV for APXPS. The XPS spectra were deconvoluted with the software UNIFIT 2013. The peak area uncertainties were carefully analyzed according to R. Hesse et. al. [1].

The XAS spectra were recorded at TLS beamline 09A2. The incident angles of the linearly polarized undulator radiation were 0° and 45° with respect to the graphene surface normal. We recorded the sample current to obtain the XAS spectra in the total-electron-yield mode. All XAS spectra were recorded in on-the-fly scan mode to prevent radiation damage. The photon energy was calibrated

against the $1s-\pi^*$ resonance of HOPG at 285.5 eV.

A QCM was used to determine the Ti coverage, as a QCM has a narrow resonance that leads to highly stable oscillations and great accuracy, even in the case of minute coverages. To duplicate the deposition conditions, we placed the QCM in front of the Ti evaporator at the same distance, deposition angle and base pressure as the sample.

References

1. Hesse, R., Chassé, T., Streubel, P., and Szargan, A. R. Error estimation in peak-shape analysis of XPS core-level spectra using UNIFIT 2003: how significant are the results of peak fits? *Surf. Interface Anal.* **36**, 1373 (2004)

2. Band diagrams measured by ARPES on bilayer graphene (BLG) and H₂-exposed BLG (without Ti).

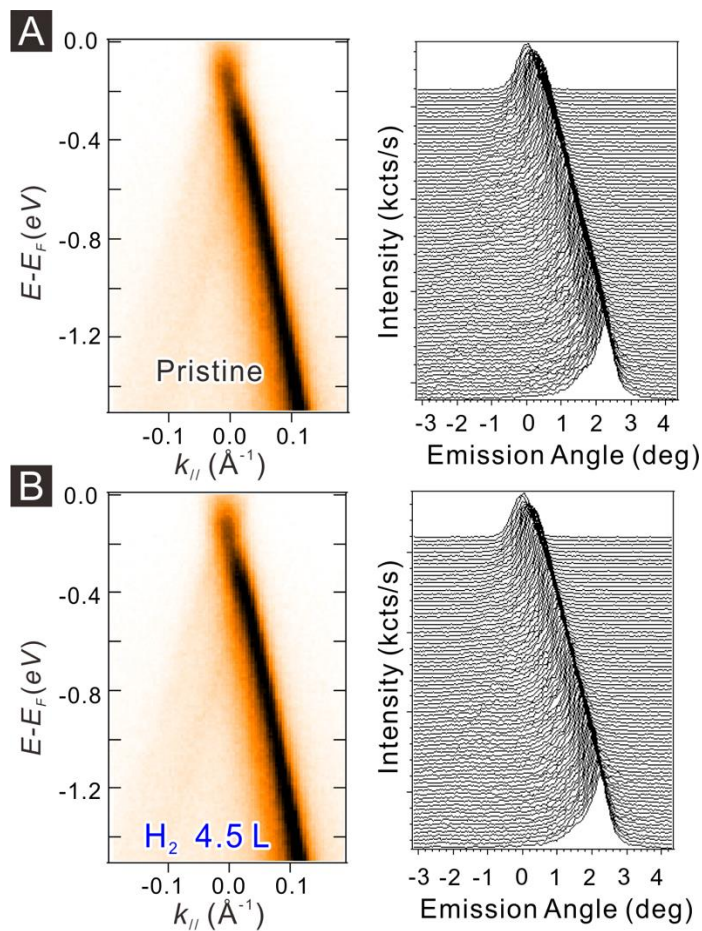


Figure S1: ARPES (left) and MDC (right) measured on (A) pristine bilayer graphene and (B) after exposure to 4.5 L of molecular hydrogen. No Ti was deposited prior to hydrogenation. The results show that the addition of molecular hydrogen near 300 K does not alter the band structure of bilayer graphene (without Ti).

3. Summary of experimental hydrogen storage capacity in graphene

Table S1

Table 1

Summary of experimental hydrogen storage capacity in graphene

H source	support	catalyst	T (k)	Pressure	Capacity (% and wt %)	Ref.
H ₂ plasma	Exfoliated graphene	No	RT	1 torr	16.67 %	1
H ₂ plasma	CVD graphene	No	RT	0.015 torr	33 %	2
H ₂ plasma	CVD graphene	No	RT	0.01 torr	25 %	3
cracked H ₂	CVD graphene on Ni (111)	No	RT	1.5×10 ⁻⁶ torr	25 %	4
cracked H ₂	CVD graphene on Ni (111)	No	RT	1.5×10 ⁻⁶ torr	25.6 %	5
cracked H ₂	CVD graphene on Ni (111)	No	RT	1.5×10 ⁻⁹ torr	25 %	6
H ₂	Exfoliated graphene	No	RT	6 MPa	0.2 wt %	7
H ₂	Graphene powder	No	RT	10 bar	0.72 wt %	8
H ₂	Nitrogen-doped graphene	Pd	RT	4 MPa	4.4 wt %	9
H ₂	Nitrogen-doped graphene	Pd NPs	RT	2 MPa	1.9 wt %	10
H ₂	Nitrogen-doped graphene	Pd NPs	RT	4 MPa	4.3 wt %	11
H₂	Crystalline graphene on SiC (0001)	Ti	RT	1 mbar (1 hr)	13.5 % 1.11 wt %	This work

References:

1. Luo, Z., Yu, T., Kim, K. J., Ni, Z., You, Y., Lim, S. Shen, Z. Wang, S., and Lin, J. Thickness-dependent reversible hydrogenation of graphene layers. *ACS Nano* 3, 1781 (2009)
2. Gowda, P., Mohapatra, D. R., and Misra, A. Enhanced photoresponse in monolayer hydrogenated graphene photodetector. *ACS Applied Materials & Interfaces* 6, 16763 (2014)
3. Son, J., Lee, S., Kim, S. J., Park, B. C., Lee, H. K., Kim, S., Kim, J. H., Hong, B. H., and Hong, J. (2016). Hydrogenated monolayer graphene with reversible and tunable wide band gap and its field-effect transistor. *Nat. Commun.* 7, 13261 (2016)
4. Lizzit, D., Trioni, M. I., Bignardi, L., Lacovig, P., Lizzit, S., Martinazzo, R., and Larciprete, R. Dual-route hydrogenation of the graphene/Ni interface. *ACS Nano* 13, 1828 (2019)

5. Haberer, D., Giusca, C. E., Wang, Y., Sachdev, H., Fedorov, A. V., Farjam, M., Jafari, S. A., Vyalikh, D. V., Usachov, D., Liu, X., Treske, U., Grobosch, M., Vilkov, O., Adamchuk, V. K., Irle, S., Silva, S. R., Knupfer, M., Büchner, B., and Grüneis, A. Evidence for a new two-dimensional C₄H-type polymer based on hydrogenated graphene. *Adv. Mater.* 23, 4497 (2011)
6. Haberer, D., Vyalikh, D. V., Taioli, S., Dora, B., Farjam, M., Fink, J., Marchenko, D., Pichler, T., Ziegler, K., Simonucci, S., Dresselhaus, M. S., Knupfer, M., Büchner, B., and Grüneis, A. Tunable band gap in hydrogenated quasi-free-standing graphene. *Nano Letters* 10, 3360 (2010)
7. Ma, L. P., Wu, Z. S., Li, J. Wu, E. D., Ren, W. C. and Cheng, H. M. Hydrogen adsorption behavior of graphene above critical temperature. *Int. J. Hydrogen Energy* 34, 2329 (2009).
8. Srinivas, G., Zhu, Y., Piner, R., Skipper, N., Ellerby, M., and Ruoff, R. Synthesis of graphene-like nanosheets and their hydrogen adsorption capacity. *Carbon* 48, 630 (2010)
9. Parambath, V. B., Nagar, R., and Ramaprabhu, S. Effect of nitrogen doping on hydrogen storage capacity of palladium decorated graphene. *Langmuir* 28, 7826 (2012)
10. Vinayan, B. P., Sethupathi, K., and Ramaprabhu, S. Facile synthesis of triangular shaped palladium nanoparticles decorated nitrogen doped graphene and their catalytic study for renewable energy applications. *International Journal of Hydrogen Energy* 38, 2240 (2013)
11. Vinayan, B. P., Nagar, R., and Ramaprabhu, S. Solar light assisted green synthesis of palladium nanoparticle decorated nitrogen doped graphene for hydrogen storage application. *J. Mater. Chem. A* 1, 11192 (2013)

4. Carbon *K*-edge XAS spectra

Polarization-dependent carbon *K*-edge XAS spectra taken with different soft X-ray incident angles relative to the surface normal are shown in Figure S2. For well-ordered systems, the polarization-dependent XAS can serve to probe the orientation of molecular orbitals [1,2]. The resonance intensity associated with a particular molecular orbital is largest when the electric field of the incoming light is parallel to the direction of the orbital, and is minimized when the field is perpendicular to the orbital. Namely, normal incident soft X-rays (i.e., 0° with respect to the surface normal) are only sensitive to in-plane orbitals, whereas 45° incident soft X-ray are sensitive to both in-plane and out-of-plane orbitals. Since the π orbital of the graphene sheet is perpendicular to the surface, only the spectra with 45° incidence can reveal the π^* resonance.

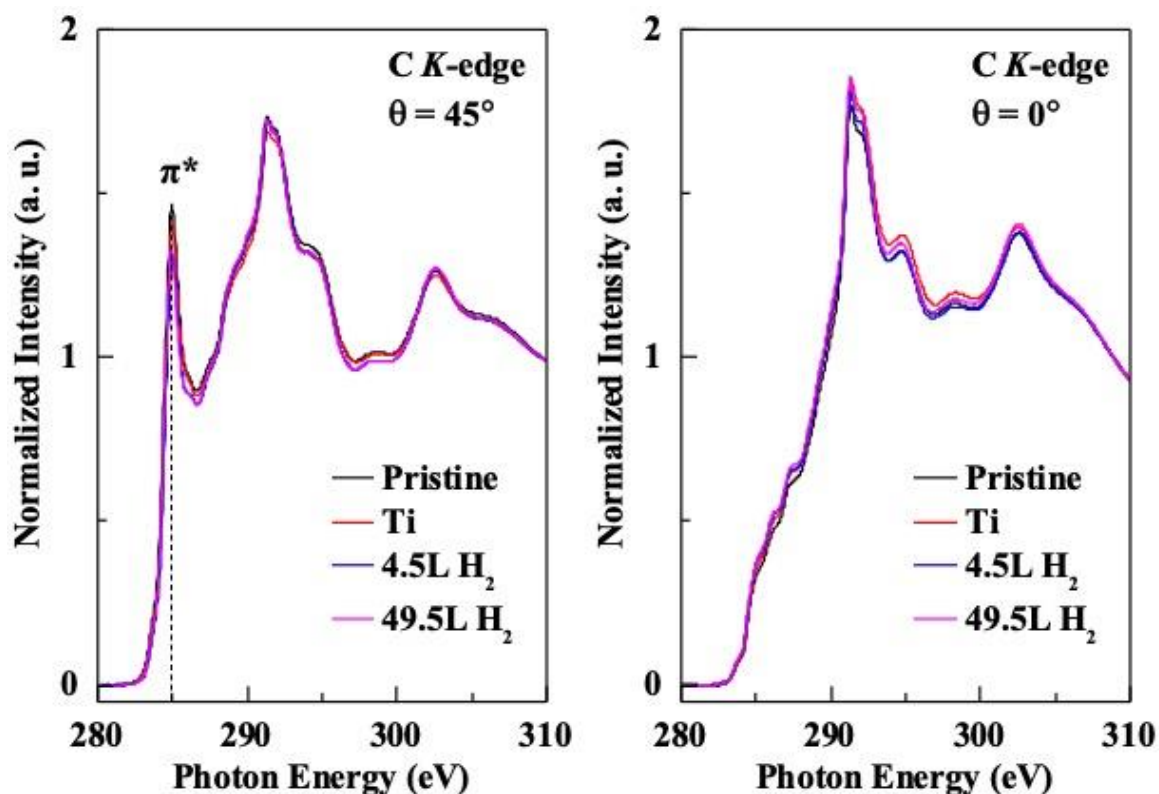


Figure S2: The full range XAS spectra of pristine graphene, Ti doped, low H_2 dosage (4.5L), and high H_2 dosage (49.5L) samples. The indicated angles are the angles of the incident soft X-ray beam relative to the surface normal.

Further, by taking the spectral difference, i.e., the 45° spectra minus the 0° spectra, we will effectively select the out-of-plane orbital alone. Figure S3 shows the difference spectra ($45^\circ - 0^\circ$) of the π^* resonance region, for pristine, Ti-doped (~ 0.03 ML), and H_2 -dosed (~ 4.5 to 49.5 L) graphene. A pronounced asymmetric π^* resonance as a spectral feature is clearly visible at about 285.5 eV. Its intensity decreases significantly with increasing H_2 dosage. This result indicates the formation of C-H bonds that suppress the number of π orbitals.

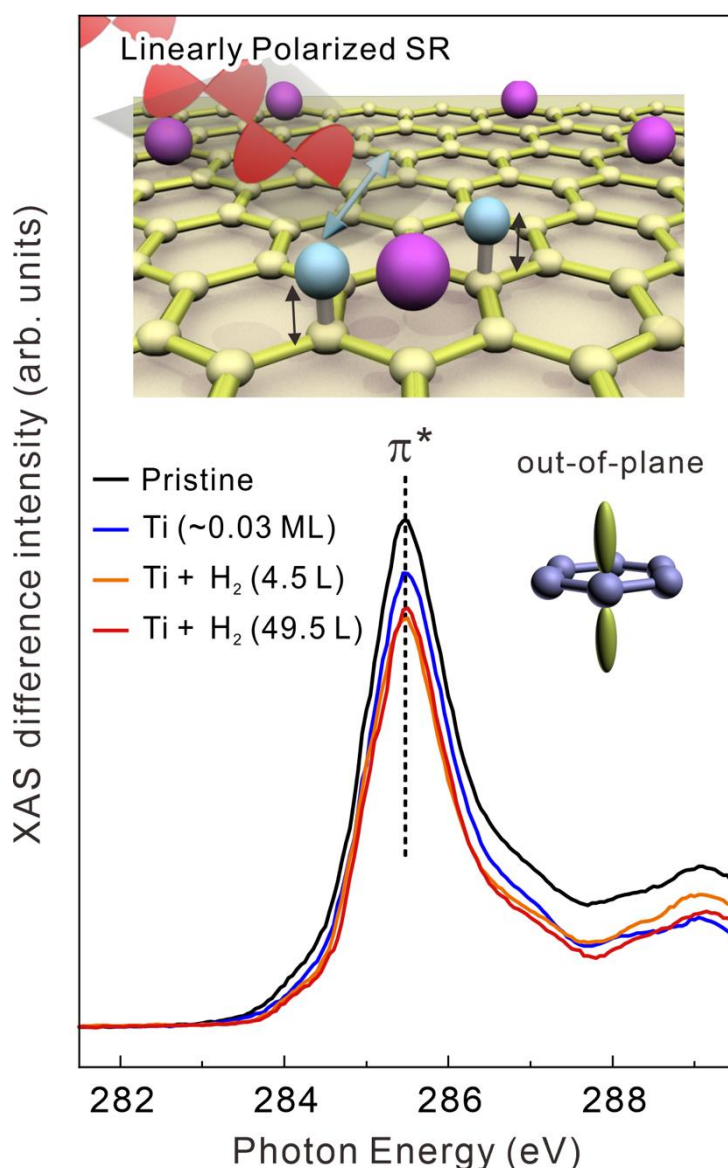


Figure S3: Carbon K-edge X-ray absorption spectra measured with linearly polarized soft X-rays on pristine graphene, after Ti deposition (Ti ~ 0.03 ML), and after exposure to molecular hydrogen

H₂ (4.5 and 49.5 L). We recorded the XAS spectra at 0° and 45° relative to the surface normal (see Fig. S2). The difference spectra (45°-0°) are presented here. The schematic diagram shows the resonance characteristics corresponding to a C-C π orbital (~ 285.5 eV) on graphene.*

References

1. Chang, L. Y., Kuo, Y. C., Shiu, H. W., Wang, C. H., Lee, Y. C., Yang, Y. W., Gwo, S. and Chen, C. H. n-Alkanethiols directly grown on a bare Si (111) surface: from disordered to ordered transition. *Langmuir* 2017 **33**, 14244-14251.
2. Lou, J. L., Shiu, H. W., Chang, L. Y., Wu, C. P., Soo, Y. L., and Chen, C. H. Preparation and characterization of an ordered 1-dodecanethiol monolayer on bare Si (111) surface. *Langmuir* 2011 **27**, 3436-3441.

5. H storage capacity of Ti SACs and Ti nanoclusters of different size on graphene

a. For a single-site Ti atom catalyst,

$$0.03 \text{ ML} = 4.0 \times 10^{13} \text{ cm}^{-2}$$

$$\eta_H = \frac{H}{C} = \frac{6 \times (4.0 \times 10^{13})}{3.8 \times 10^{15}} \times 100\% \approx 6.3\%$$

b. For a single-site Ti nanocluster catalyst,

Table S2: Details of calculation of hydrogen storage capacity

Number N of Ti atom in nanoclusters of different size [1]	Nanocrystal Radius R_c (nm) [2]	Diffusion area (nm ²)	H storage amount	H storage per Ti atom
10	0.251	0.229	25	2.5
38	0.502	0.655	41	1.079
95	0.753	1.081	57	0.6
192	1.005	1.507	73	0.38
339	1.256	1.933	90	0.265
547	1.507	2.359	106	0.194
826	1.758	2.785	122	0.148
1187	2.009	3.211	138	0.116
1640	2.26	3.638	154	0.094
2196	2.511	4.064	171	0.078

Hydrogen storage amount is calculated as H storage amount = Diffusion area \times C–H site density

H storage per Ti atom is calculated as H storage per Ti atom = $\frac{\text{Diffusion area} \times \text{C–H site density}}{N}$

References

1. Martin, T. P. Shells of atoms. *Phys. Reports* 1996 4, 199-241.
2. Duncan Lyngdoh, R. H., Schaefer III, H. F., and King, R. B. Metal–metal (MM) bond distances and bond orders in binuclear metal complexes of the first row transition metals titanium through zinc. *Chem. Rev.* 2018 24, 11626-11706.

6. Formation of C–H bonds on graphene/SiC and its identification using APXPS

From the integrated area of the Gr1 component, we can determine the hydrogen coverage (in %) of crystalline graphene with Ti nanocluster catalysts.

Table S3 Summary of fitting peak position, relative intensity, and relative area of every peak of the C 1s APXPS spectra (pristine, Ti, and Ti+H₂) after baseline subtraction.

	peak	Position (eV)	Intensity (a.u.)	Area
Pristine	Gr	284.4	56141.7	80760
	B	283.4	57071.4	70301
	S1	284.7	9098.9	24696
	S2	285.2	32528.5	46114
Ti	Gr	284.5	36700.0	52768
	B	283.3	37000.6	47492
	S1	284.8	5982.1	16239
	S2	285.1	22000.2	31193
Ti+H₂	Gr	284.4	20000.0	22187
	B	283.3	27600.1	34834
	S1	284.7	4500.1	11563
	S2	285.1	16499.9	23302
	Gr1	285.0	5100	5378
	Gr2	284.1	15000	12189